MULTIPACTOR STUDIES FOR DIAMOND STORAGE RING CAVITIES

S. A. Pande, M. Jensen, Diamond Light Source Ltd., Oxfordshire, U.K.

Abstract

The Diamond storage ring is presently operating with two CESR type Superconducting (SC) RF cavities operating at 499.654 MHz. The cavities are suffering from a significant number of trips due to a sudden loss of accelerating field believed to be caused by multipacting. It is observed that operating the cavities at lower voltages reduces the trip frequency significantly. In order to estimate the multipacting thresholds and to determine safe (multipactor free) parameter zones, we have initiated a detailed simulation study of multipacting in the cavities and the coupling waveguide. The cavities have fixed coupling, and therefore the match of the cavities varies with beam current, radiation loss and cavity voltage. A change in any of these parameters leads to a different standing wave in the waveguide. This requires the simulations to account for the different operating conditions. In addition to the waveguide and the cavity cell, the simulations also indicate the possibility of multipactor in the connecting beam tubes. In this paper, we summarise the results of our simulations obtained using CST Studio PIC and Tracking solvers.

INTRODUCTION

Diamond has suffered with frequent trips interrupting beam operation. The trips result in a sudden loss of accelerating field followed by a large pressure spike observed on the gauges placed on the beam pipes and in the vicinity of the RF window (PO Box). Despite regular cavity conditioning [1], the trip rate remained unacceptably high, so we initiated a detailed multipactor simulation study of the cavity and the waveguide.

The Diamond cavities are single cell elliptical cavities with relatively large diameter beam tubes to facilitate the propagation of the HOMs to loads mounted outside the cryostat. The RF power is transmitted through rectangular waveguide WR1800. Inside the cryostat, the height of the waveguide is reduced. The reduced height waveguide on the cavity end opens up in the RBT and couples RF power into the cavity through a specially shaped iris (with a protrusion from the broad wall known as the 'coupling tongue') as shown later in Fig. 9. Figure 1 shows the RF cavity and its different parts as modelled in CST Studio [2]. The niobium parts are shown in a bluish colour. The stainless steel thermal transitions and the reduced height waveguide is copper plated to reduce the RF losses. These parts are shown in a reddish colour. The RF window and the rest of the waveguide are shown in grey.

Like other SC cavities, the Diamond/CESR cavities are elliptically shaped to reduce the possibility of one point or single surface multipacting in the main cavity body. Secondary electrons, generated at the high E field

_____
*Shivaji.pande@diamond.ac.uk

locations, drift towards the equator of the cavity due to the varying magnetic field along the cell wall losing energy on successive impacts. The E field vanishes at the equator, reducing the energy gain by the secondary electrons to a minimum and thus arresting one point multipactor [3]. However, there is still a significant possibility of two point multipacting in elliptic cavities near the equator [4]. Though the electric field vanishes at the equator, the strong magnetic field near the equator bends the path of the electrons causing them to strike the cavity surface on either side of the equator, where the surface electric field is non-zero and its amplitude is in the range favourable for MP to take place.
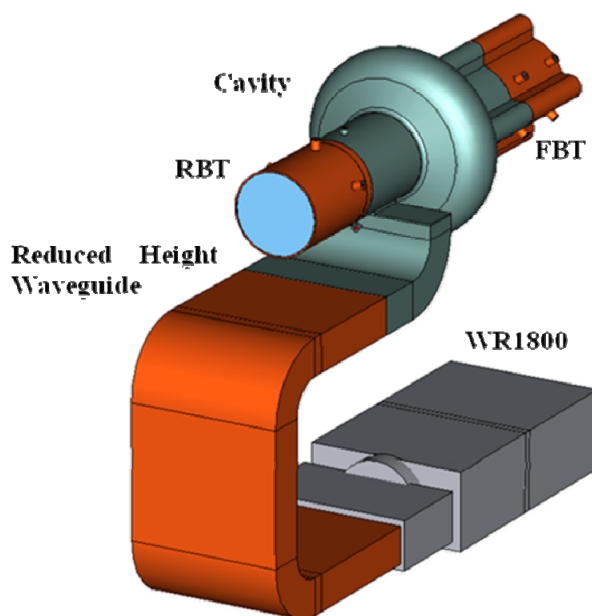

Figure 1: The Diamond storage ring cavity and the coupling waveguide as modelled in CST Studio.

In addition to the main cavity body, the other regions, where multipacting can be suspected to occur, are the reduced height waveguide, the region around the coupling tongue and the beam tubes. Multipacting in the reduced height waveguide has been studied at Cornell and at Daresbury Laboratory [5,6]. As a result of these studies, certain remedies were suggested to reduce the multipactor in the waveguide [7]. These include coating the waveguide with TiN, longitudinal grooves and ridges in the centre of the waveguide broad wall and the use of a longitudinal DC bias magnetic field, to distort the path of the multipacting electrons. Waveguides with single and multiple grooves were investigated and it was found that these can reduce the multipactor saturation current and decrease the growth rate but they cannot prevent it.

The Diamond cavities have been provided with the anti-multipactor coils on the waveguide. However, this method will only be effective for the copper plated parts of the waveguide as these coils rely on the magnetic field penetrating into the waveguide wall to disturb the electron trajectories.

For the present study, we concentrate on multipacting in main cavity body, region about the coupling tongue, some parts of the reduced height waveguide and the beam tubes.

MULTIPACTOR MODELLING

Since the cavities are greatly over coupled, the power reflected from the cavities, and thus the standing wave pattern in the waveguide, depends strongly on the operating parameters such as the stored beam current and the voltage across the cavity. During cavity conditioning, almost all of the power is reflected, resulting in a strong standing wave in the waveguide. On the other hand, the cavities are perfectly matched at certain beam power and voltages. Under these conditions, the fields in the waveguide will form an almost perfect travelling wave (TW). Additionally, to minimise the reflected power, we use a 3-stub tuner to match the cavities during the non-optimal conditions of operation. Therefore, to investigate these conditions, we considered the following representative cases.

a) A cavity with full reflection – strong SW in the waveguide

b) A perfectly matched cavity – almost perfect TW in the waveguide

c) A cavity with some reflection – partial SW in the waveguide

d) A cavity operating with the 3-stub tuner – SW between cavity and 3-stub tuner

EM Fields for Multipactor Simulation

To study the multipacting in the cavity and the waveguide, we need to obtain EM fields which are representative of the actual operating conditions. The EM fields inside the cavities are mainly in a standing wave regime, whereas, depending on the operating parameters, those inside the waveguide can either be in SW or in TW mode.

To obtain SW or TW fields in a section of waveguide is straight forward and these can be obtained from a TD or a FD solver run. However, to obtain steady state TW or SW fields in a waveguide coupled to a cavity, TD/FD solvers with losses must be used. As the Diamond/CESR cavities are excessively over-coupled for high current operating conditions, normal time domain solution will always yield a SW in the waveguide with full reflection. To obtain a steady state field in TD, one must wait for the energy in the calculation domain to decay sufficiently. It can also be obtained by a monochromatic excitation of the cavity at the resonant frequency. In such a case, one must wait for

the fields to reach the steady state value, which takes a few filling times (100s of μs compared to a 2 ns RF cycle). Such simulations are very time consuming, however the FD solver reaches steady state relatively fast.

To obtain the *representative* SW field in the cavity and TW or partial SW field in the waveguide numerically, we simulated the cavity as a *one port* device. Without disturbing the coupling iris, we changed the conductivity of the niobium part of the cavity and the waveguide. We know

$$Q_{ext} = \frac{Q_0}{\beta} \text{ or } \beta = \frac{Q_0}{Q_{ext}}$$

If Q_0 and Q_{ext} (or β) are known at one conductivity σ_1, we can estimate these values for any other conductivity σ_2. Alternatively, the conductivity can be estimated for any desired value of Q_0 or β using

$$\frac{Q_{01}}{Q_{02}} = \frac{\beta_1}{\beta_2} = \sqrt{\frac{\sigma_1}{\sigma_2}}$$

We used the measured values of Q_0 and β at room temperature and used the conductivity of normal conducting niobium to get the conductivity to obtain the fields with desired values of S11 or VSWR corresponding to the operating parameters.
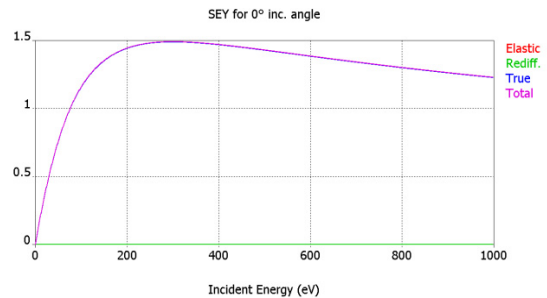

Figure: 2 SEY for 'Niobium 300°C Bakeout' as used in CST Studio

SEE Properties

CST Studio uses Furman-Pivi probabilistic model for secondary electron emission [8]. There are several secondary electron emitting materials available in the material library of CST Studio including copper, copper (ECSS), niobium etc. SEE properties of niobium are available for three different surface treatments namely 'Wet Treatment'(Nb-WT), '300°C Bakeout' (Nb-300DB) and 'Ar Discharge Cleaned' (Nb-ArDC). Figure 2 shows SEY (Secondary Electron Yield) denoted by 'δ' of 'SEE Niobium - 300°C Bakeout' as a function of impact energy of electrons. It has $\delta_{max} = 1.49$ at $E_{max} = 300$ eV. Nb-WT has $\delta_{max} = 2.8$ at $E_{max} = 230$ eV and the corresponding values for Nb-ArDC are 1.25 and 342 eV respectively. Material properties of Nb-WT and 300DB are used for most of the simulations summarised below. Since the

waveguide and the thermal transitions are plated internally with copper, SEE properties of copper (ECSS) are used for these parts. The parameter *'maximum number of generations'* has been set to 1000.

RESULTS

In order of severity, the major suspected regions of the cavity, where multipacting can occur, are the main cavity cell, the coupling tongue, the waveguide and the beam tubes. To concentrate on individual parts, simulations with appropriate fields and primary electrons confined to those particular parts were performed.

Multipacting in FBT

There is very strong electric field in the beam tubes, especially in the regions near the main cavity cell. Figure 3(a) shows the E field of the TM010 mode in a transverse section trough the FBT. It can be seen that, near the axis the field is mostly in the longitudinal direction and any electrons generated or entering this region, will be accelerated longitudinally and will escape the cavity through the beam tubes or collide with the wall with an increased energy. The field near the beam tube wall is predominantly transverse, and can accelerate electrons entering this region towards or away from the wall depending on the phase. Figure 3(b) shows the E field inside the cylindrical part of one of the flutes at the same z location as that of Fig. 3(a). The field amplitude varies from a few tens to few hundreds of keV/m along the surface. This field configuration and the geometry of the flutes (especially the flute shoulders) can provide favourable conditions for multipactor.
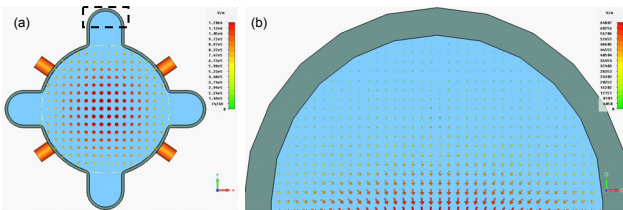

Figure 3: (a) A transverse section through FBT at z = -62.5 mm showing the electric field of the TM010 mode. (b) Close up of the top part of the top flute shown by dotted rectangle in (a).

PIC simulations are carried out for three different material choices (a) Nb–WT, (b) Nb-300°C Bakeout and (c) Nb–Ar Discharge cleaned. Primary electrons are generated in a cuboid in the Nb part of the bottom flute. The electrons are released at regular intervals, over the whole RF cycle, at random positions within a cuboid in the lower flute, to cover a significant part of the probable locations which may lead to multipactor. Figure 4 shows the growth in the number of electrons with time for material Nb-WT. The cavity voltage is varied from 1.44 MV to 1.57 MV in 0.026 MV steps. As can be observed, for cavity voltage ≥ 1.49 MV, there is exponential growth in the number of electrons. It is also seen that the growth is faster at higher voltages. The inset

shows the graph details for time between 350 and 360 ns for cavity voltage of 1.57 MV. This indicates that the multipacting in flutes is a single surface or one point multipacting. Above 1.6 MV, multipacting is always observed in the flutes. The maximum number of secondaries per hit is limited to 3. Figure 5 shows multipacting electrons in the lower flute for material choice Nb-WT at 1.57 MV. The maximum electron energy is clamped to 200 eV in this picture which indicates that most of the impacting electrons have energies lower than 100 eV.
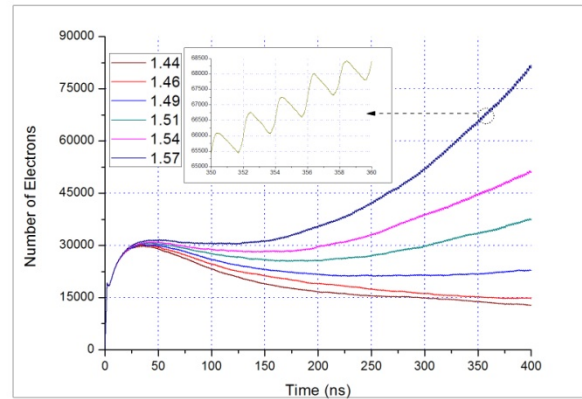

Figure 4: The number of electrons vs time (ns) for primary electron source inside one of the flutes for material choice Niobium – Wet Treatment and cavity voltage varied from 1.44 to 1.57 MV. The inset shows the graph details for time between 350 and 360 ns for cavity voltage of 1.57 MV.
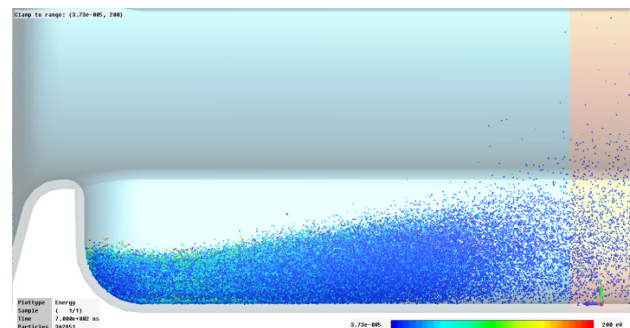

Figure 5: Multipactor in the flute at 1.57 MV for material Niobium - Wet Treatment. The maximum electron energy clamped at 200 eV indicates that most of the impacting electrons have energies below ~100 eV.

Similar several runs were dedicated to material choice of Nb-300DBk and Nb-ArDC. The multipacting could not be observed for cavity voltage scanned from 0.5 to 3.7 MV even with very large number of primary electrons. Observation of SEE characteristics for Nb-WT shows that $\delta > 1$ at energies as low as ~35 eV. Whereas $\delta > 1$ for energies ~80 and ~125 eV for materials Nb-300DB and Nb-ArDC respectively. Therefore, the multipacting in the FBT will represent a weak barrier and may be observed

only in an unconditioned or a 'raw' cavity. This might be conditioned out very easily.

Multipacting in the Cavity

As mentioned earlier, the cavity equator provides the most favourable conditions for two point multipacting. Any electrons generated in the off-axis region are most likely to be accelerated towards one of the side walls due to the strong electric field. The secondaries generated on the cavity wall drift towards the equator on successive impacts. A strong magnetic and moderate electric field about the equator make the conditions favourable for two point multipactor.
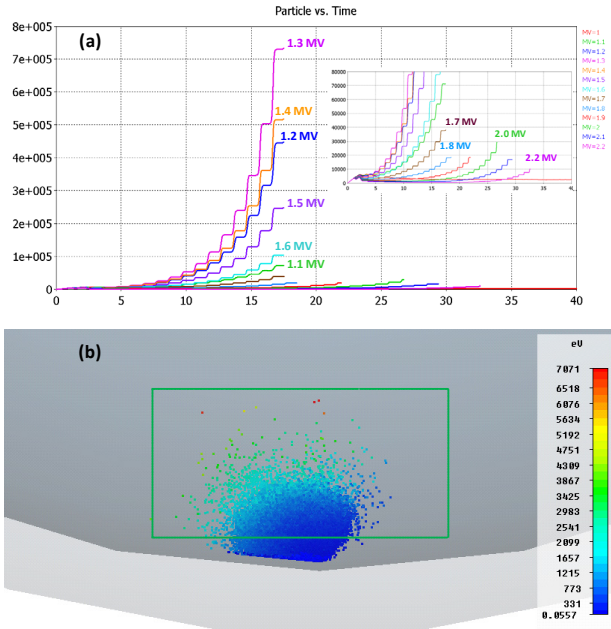

Figure 6: Multipacting near the equator for material choice Nb-300DB. (a) Number of electrons vs time (ns) for cavity voltages 1 to 2.2 MV. The inset shows a close up of the curves for 1.7 to 2.2 MV. (b) A well formed multipacting bunch at 17.5 ns for 1.3 MV.

To prevent the number of secondaries from growing excessively large and to avoid multipacting at multiple locations azimuthally along the equator, we limited the primary electrons to a very small volume near the equator. PIC simulations were carried out for three material choices of niobium as described above. Figure 6 shows the multipacting characteristics near the equator for material choice Nb-300DB. Fig. 6(a) shows the number of electrons vs time for cavity voltages between 1.0 and 2.2 MV in 0.1 MV steps. The inset shows the close up for 1.7 to 2.2 MV. As seen, the growth rate increases as the cavity voltage is increased from 1.0 up to 1.3 MV but reduces as the cavity voltage is increased further. Figure 6(b) shows a well formed multipacting bunch at 1.3 MV. The green rectangle shows the volume in which 361 primary electrons were generated over 1 full RF period to start with in each case.

In order to compare the risk of multipacting at different voltages, we calculate the 'effective' average secondary emission coefficient (SEC) $\langle\delta_{eff}\rangle$ as follows. Careful observation of the curves and the particle monitor data, reveals that it is a two point multipacting of order *one* (higher order multipacting may occur at voltages below 1 MV). The secondaries impact twice every rf period (T_{RF}) or every 2 ns. The multipacting is detected in CST Studio by detecting the exponential increase in number of secondaries. It checks if the slope of the curve for secondaries vs time, is greater than a user defined exponential factor at three successive interval boundaries and their midpoints. Additionally, starting with *n* primary particles, at least *n* secondary particles must be created at the midpoint of the following interval for multipactor to occur. Let t_0 denote the interval width and t_{MP} be the time at which multipacting is detected. The number of impacts occurring in time t_0 will be $n_{imp} = 2t_0/T_{RF}$. In each case, we take the number of particles at $t = t_{MP} - 3t_0$ as the starting number denoted by n_s. Then $\langle\delta_{eff}\rangle$ is calculated as

$$\langle\delta_{eff}\rangle = \left(\frac{n_{MP}}{n_s}\right)^{(1/3n_{imp})}$$

where n_{MP} is the number of particles at $t = t_{MP}$. We always start with a single particle at $t = t_{MP} - 3t_0$.
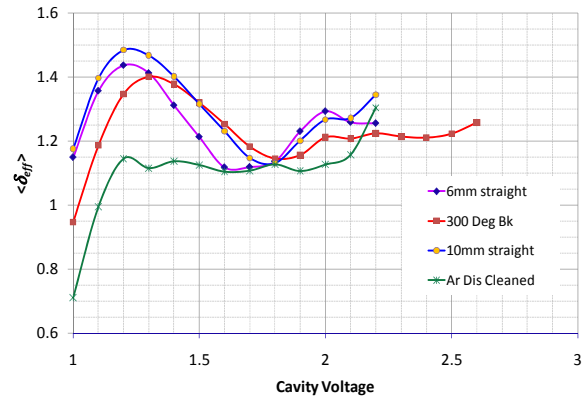

Figure 7: $\langle\delta_{eff}\rangle$ vs cavity voltage for Nb-300DB and Nb-ArDC. Two additional curves are included for 6 and 10 mm straight sections placed at the equator for material Nb-300DB.

Figure 7 shows the variation of $\langle\delta_{eff}\rangle$ with the cavity voltage for two materials Nb-300DB and Nb-ArDC. We investigated the effect of a slight deviation of the geometry from a perfect circular arc by introducing a small straight section at the equator. The effect of adding straight sections of 6 and 10 mm are shown by pink and blue curves respectively in Fig. 7. It can be observed that $\langle\delta_{eff}\rangle$ reaches a maximum at 1.3 MV and minimum in the range of 1.6 – 1.8 MV and rises again at 2 MV. This may be due to the geometry at the equator which may need further investigation. Figure 8(a) shows the collision current with the cavity shell from PIC solver for cavity voltages from 1.1 to 2.1 MV. The time axis is adjusted so that $t = 0$ occurs at -5 ns from the centre of the last bunch

(after which multipactor is detected) in each case for the sake of comparison. The curve in Fig. 8(b) shows the bunch width (FWHM) at different voltages. It is seen that the bunch is not well formed for voltages under 1.2 MV. At ~1.3 MV the bunch is well formed, indicating that multipacting may take place over a relatively large phase and energy window. As the voltage is increased further the bunch width shrinks indicating that not many electrons find themselves in a stable energy and phase window. As we used the same distribution of primary electrons in each case, most of the electrons are lost within a few hits with the surface at higher voltages and very few electrons lead to the formation of a stable multipacting bunch. Once the bunch is formed, then the multipactor growth is very fast.
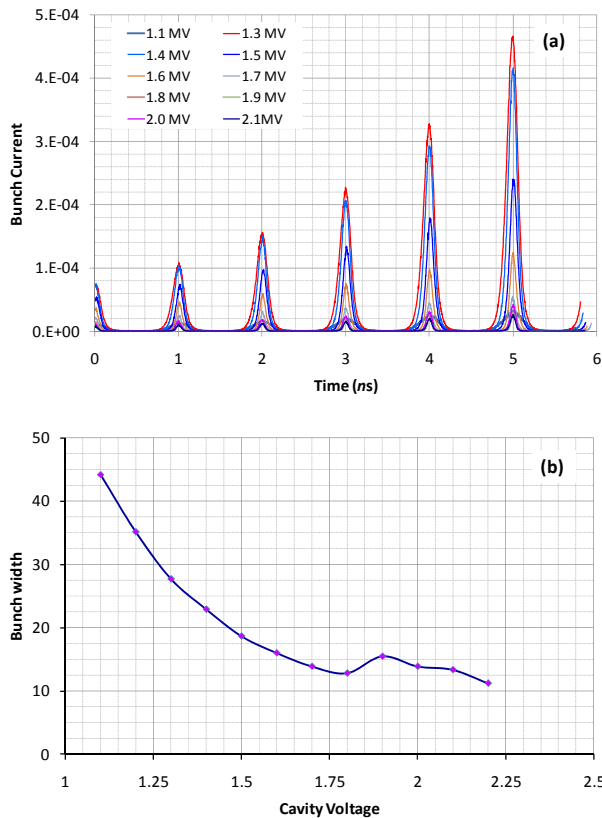

Figure 8: (a) The collision current showing the last 5 multipacting bunches for the curves shown in Fig 6(a). The time axis is shifted so that $t = 0$ occurs at -5 ns from the centre of the last bunch in each case. (b) Bunch length (FWHM) of the multipacting bunches as function of voltage (MV).

Multipacting in the Coupling Waveguide

The coupling tongue and the surrounding area is the next zone after the cavity body where strong multipacting is suspected. Eigen mode and FD simulation results reveal that the SW field from the operating mode penetrates into the waveguide well below the coupling tongue. This field near the coupling tongue is quite strong compared to that in the rest of the waveguide.
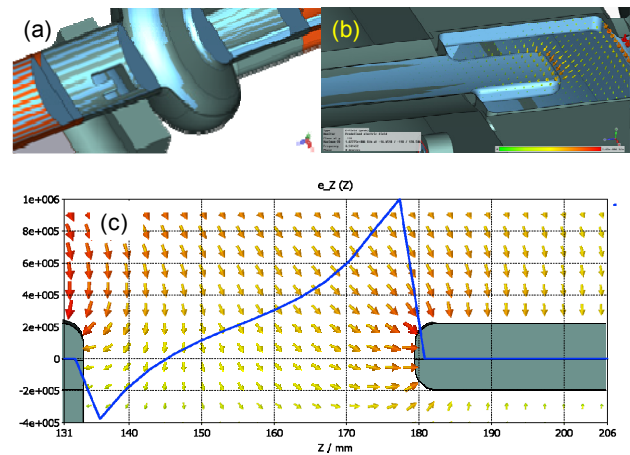

Figure 9: Details around the coupling tongue (a) geometry and (b) E field around coupling tongue. (c) A vertical section through the coupling tongue showing electric field in the gap between coupling tongue and the opposite face of the waveguide. The blue curve shows the variation of Ez along a horizontal line joining the vertical centre of the coupling tongue to the opposite face on the waveguide.
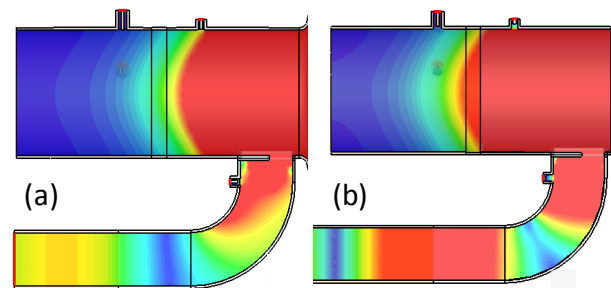

Figure 10: Electric field (Abs) in the vicinity of the coupling tongue (a) perfect TW and (b) full SW. The maximum field value is clamped at 200 V/m with input power of 0.5 W in both the cases.

The geometry and E field near the coupling tongue is shown in Fig. 9(a) and 9(b) respectively. Figure 9(c) shows the electric field at its maximum in a vertical section through the coupling tongue. It can be seen that a direct discharge or straight trajectories starting from the coupling tongue and terminating on the opposite face or vice versa is unlikely. Figures 10(a) and 10(b) show the E field magnitude in the vicinity of the coupling tongue and the nearby waveguide in perfect TW (S11 = -48 dB) and full SW (S11 = -0.013 dB) mode respectively as computed using the FD solver. It can be noted that the cavity field penetrates into the coupling waveguide even under perfect TW conditions. PIC simulations with a primary electron source on the coupling tongue tip and in the coupling iris were carried out. The simulations indicated no activity across the coupling tongue.

Multipacting characteristics for perfect TW field in the waveguide at power levels from 50 to 300 kW are shown in Fig. 11. Primary electrons are released in the coupling iris during the phase favourable for acceleration towards the waveguide. Under TW conditions, the secondaries are

swept away by the magnetic field spreading the multipacting longitudinally along the waveguide. The results reveal that higher order two point multipacting may take place in the waveguide at power levels up to ~150 kW. Additionally, due to the penetration of the SW field from the cavity, there is a strong possibility of 'one point' multipacting in the coupling waveguide just below the iris. The inset shows zoomed in part of the curve for 275 kW between 28 and 32 ns. It appears that there is an impact almost every ns indicating two point multipacting. Figure 12 depicts the particle positions from 28.5 ns to 31 ns at every 0.5 ns at 275 kW. It can be seen that there are two multipacting bunches individually impacting on the respective surfaces but 180° out of phase with respect to each other. Both bunches move in synchronism in the same direction, the left bunch making impact on the left surface at the time when the right bunch is farthest from the right surface and vice versa giving rise to the 'push-pull' multipacting.
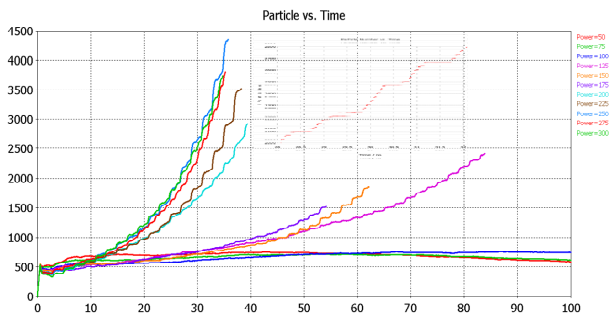

Figure 11: Number of electrons vs time for perfect TW field in the waveguide for 50 to 300 kW.
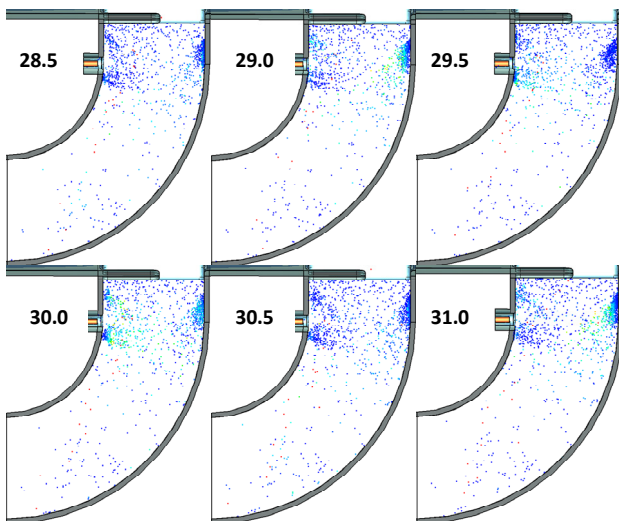

Figure 12: The 'Push-Pull' multipacting occurring just under the coupling tongue inside the coupling waveguide at 275 kW with perfect TW field. The maximum electron energy is clamped at 1 keV.

DISCUSSION AND CONCLUSION

The multipacting simulations were carried out with SW fields in the cavity cell and the FBT. The multipacting in the FBT does not pose a serious problem and is only observed for materials with a high SEY. The two point multipacting near the equator can be severe. The studies reveal that, at lower voltages typically between 0.5 and 1 MV, higher order two point multipacting can take place. As the voltage is increased above 1 MV well defined multipacting bunches start to form. At about 1.3 MV the energy and phase stable zone is the widest. Therefore the average effective secondary emission coefficient, $<\delta_{eff}>$ is maximum which results in a larger multipacting bunch involving a larger surface area about the equator. As the voltage is increased further, the multipacting bunch width shrinks and the bunches are well separated. This indicates that the multipacting is possible only in a narrow phase width and a narrow area about the equator. We could simulate some of the representative operating conditions in the waveguide. Conditions favourable for multipacting in the waveguide near the coupling tongue, due to penetration of the cavity field into the waveguide, are observed.

REFERENCES

[1] P. Gu, et. al. Reliability improvement of Diamond Superconducting Cavities; SRF2011 Conference, Chicago, IL, MOPO068 (2011).

[2] CST Studio Suite, CST AG, Dermstadt, Germany.

[3] H. Padamsee, J. Knobloch and T. Hays; RF Superconductivity for Accelerators; John Wiley & Sons, 1998, Ch. 10.

[4] V. Shemelin; Multipacting in Crossed RF Fields Near Equator, Proceedings of EPAC 2004, European Particle Accelerator Conference, Lucerne (2004), p. 1075 – 1077.

[5] R. L. Geng, H. Padamsee, V. Shemelin; Multipacting in Rectangular Waveguide, Proceedings of the 2001 Particle Accelerator Conference, Chicago (2001), p. 1228 – 1230.

[6] R. L. Geng, P. Goudket, R. G. Carter, S. Belomestnykh, H. Padamsee, D. M. Dykes; Dynamical aspects of multipacting induced discharge in a rectangular waveguide, Nuclear Instruments and Methods in Physics Research A 538 (2005), p. 189 – 205.

[7] P. Goudket; A Study of Multipacting in Rectangular waveguide; Ph. D. Thesis, Lancaster University, 2004.

[8] M. A. Furman and M. T. F. Pivi; Probabilistic model for the simulation of secondary electron emission; Physical Review Special Topics – Accelerators and Beams; Vol. 5, 124404 (2002).